MULoc: Towards Millimeter-Accurate Localization for Unlimited UWB Tags via Anchor Overhearing

Junqi Ma, Fusang Zhang, Beihong Jin, Siheng Li, and Zhi Wang
KLSS(CAS) and SKLCS, Institute of Software, Chinese Academy of Sciences, China
University of Chinese Academy of Sciences, China

IEEE INFOCOM 2025 - IEEE Conference on Computer Communications | 979-8-3315-4305-1/25/$31.00 ©2025 IEEE | DOI: 10.1109/INFOCOM55648.2025.11044652

***Abstract*—Recent years have seen rapid advancements in ultra-wideband (UWB)-based localization systems. However, most existing solutions offer only centimeter-level accuracy and support a limited number of UWB tags, which fails to meet the growing demands of emerging sensing applications (*e.g.*, virtual reality). This paper presents MULoc, the first system that can localize an unlimited number of UWB tags with millimeter-level accuracy. At the core of MULoc is the innovative use of UWB phase, which can provide finer-grained distance measurement than traditional time-of-flight (ToF) estimates. To accurately obtain phase estimates from unsynchronized devices, we introduce a novel localization scheme called anchor overhearing (AO) and eliminate raw signal errors through a signal-difference-based technique. For precise tag localization, we resolve phase ambiguity by combining a fusion-based filtering method and frequency hopping. We implement MULoc on commercial UWB modules. Extensive experiments demonstrate that our system achieves a median localization error of 0.47 mm and 90-th percentile error of 1.02 cm, reducing the error of traditional method by 91.12%.**

I. Introduction

The accurate and efficient localization for mobile devices has been a longstanding pursuit in the research community. In the era of the internet of things (IoT), it plays a crucial role in various applications such as gesture recognition [1], virtual reality (VR) [2], and motion capture (MoCap) [3]. These emerging applications typically require the localization system to offer millimeter-level accuracy and the capacity to localize numerous devices simultaneously. For instance, a MoCap system used in film and gaming needs to track multiple actors, accurately localizing hundreds of small markers across their bodies to capture detailed and complex motions. Similarly, in multiplayer VR games, the system also need to reliably track multiple controllers and helmets with high precision to ensure each motion is correctly visualized.

Prior work has made significant advances in building localization systems with various signals, including infrared optics [4], WiFi [5–14], RFID [15–17], and acoustic signals [18–20]. Although promising, optical and RFID-based solutions depend on dedicated devices [2], which are often too costly for widespread use. In contrast, WiFi and acoustic signals are more available in consumer-level devices. However, they fail to offer reliable accuracy in complex real-life scenarios [21].

Fusang Zhang and Beihong Jin are corresponding authors.

This work is partially supported by the National Natural Science Foundation of China (No.62422213, No.62172394, No. 62072450), the Beijing Nova Program, the Beijing Natural Science Foundation (L223034), the Innovation Team 2024 ISCAS (No. 2024-66), and the Basic Research Program of ISCAS (No. ISCAS-JCMS-202305).

Recently, ultra-wideband (UWB) technology has gained popularity due to its widespread adoption in consumer-level devices such as smartphones [22]. Benefiting from a large bandwidth of 500 MHz, UWB signal can provide centimeter-level localization accuracy, superior to other signal modalities. Existing UWB-based localization systems can generally be divided into two categories: time-based [23–29] and angle-based [30–36]. Time-based systems typically involve multiple anchors with known locations, each estimating the time-of-flight (ToF) from the UWB tag. The tag's location can then be determined by combining multiple ToF estimates using trilateration [37]. However, the limited precision of ToF estimates fails to offer millimeter-level localization accuracy. In contrast, angle-based methods use an antenna array to measure the angle-of-arrival (AOA) of signals sent from tags. Single-anchor localization can be achieved by fusing the ToF and AOA estimates [38]. However, these solutions typically exhibit large errors of over 10 cm due to the limited number of antennas (*i.e.*, 2 or 3) on commercial devices [33]. Novel systems such as ATLAS [24] and SnapLoc [25] utilize time-difference-of-arrival (TDOA) scheme to support localization for an large number of UWB tags. However, the accuracy of this approach are still limited to centimeter-level due to the errors in ToF estimates.

This paper presents MULoc, the first system capable of localizing an unlimited number of UWB tags with millimeter-level accuracy. Unlike traditional TDOA systems that rely only on coarse-grained ToF estimates, MULoc leverages precise UWB phase for fine-grained tag localization. Benefiting from the high phase resolution of 0.02 rad available on commercial UWB devices [33], millimeter-level distance resolution can be achieved by quantifying the relationship between signal phase and path length. While promising, there are two critical challenges need to be addressed before implementing MULoc.

The first challenge is **how to acquire accurate phase estimates from unsynchronized UWB devices**. Due to the lack of synchronization and varying antenna delays among separate anchors and tags, the raw UWB signals exhibit severe time-varying errors including carrier frequency offset (CFO) and initial offset, which cannot be directly used for localization. Although some prior work [39–42] explores the use of bi-directional ranging packets between the anchors and tags to cancel out these errors, this method suffers from severe packet collision when numerous tags are present. MULoc addresses this issue by introducing a novel scheme called

anchor overhearing (AO). In the AO scheme, anchors sequentially broadcast UWB packets, which are overheard by both tags and other anchors in the listening state. We observe that these signals overheard by tags and anchors from the same transmitter contain similar errors. Leveraging this insight, we propose a signal-difference-based processing method to fully remove the errors in the raw UWB signal and obtain accurate ToF and phase estimates.

With the recovered UWB signal, we then face the second challenge: **how to achieve fine-grained tag localization with UWB phase estimates**. To perform trilateration, it is essential to accurately measure the distance differences between the tag and multiple anchors. However, due to phase wrapping, the distance measured from the UWB phase contains an unknown number of whole wavelengths. Additionally, owing to the large random noise and tag-location-dependent bias in ToF estimates, we cannot directly use them to resolve the phase ambiguity. To address this issue, we first propose to reduce the random noise of ToF estimates by employing a fusion-based filtering method combining ToF and accurate relative phase change. We further enhance the robustness of ambiguity resolution by performing frequency hopping to combine the phase estimates with different wavelengths.

We implement MULoc using commercial DW1000 UWB module. Extensive experimental results demonstrate that MULoc achieves a median localization accuracy of 0.47 cm, reducing the error by 91.12% compared to the traditional TDOA-based method. The contributions of this paper are summarized as follows:

- To the best of our knowledge, MULoc is the first system that can localize an unlimited number of UWB tags with millimeter-level accuracy.
- We propose a novel anchor overhearing scheme for UWB localization and a signal-difference-based recovery method, which can provide accurate phase estimates in practical localization scenarios.
- We introduce a fusion-based filtering method and use frequency hopping to enhance phase ambiguity resolution.
- We implement MULoc on commercial UWB devices using the proposed anchor scheduling scheme and evaluate its performance with extensive experiments. We also release our source code to facilitate further research in this field.

II. MULoc Overview

To help understand MULoc's key innovations, this section compares its unique anchor overhearing scheme with the traditional TDOA method. We also provide an overview of MULoc's signal processing pipeline.

A. Localization Scheme

TDOA scheme. Early UWB localization systems mostly rely on the two-way ranging (TWR) scheme, where tags perform two-way ranging with all anchors in the system. Although straightforward, this method requires numerous packet exchanges, leading to severe packet collisions when many tags

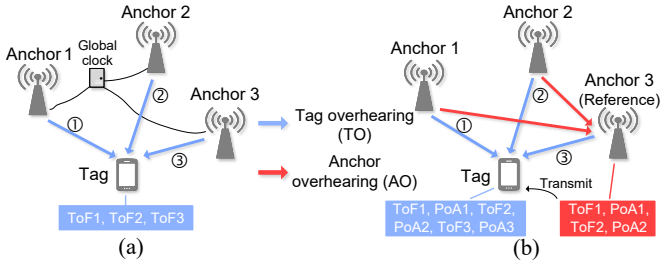

Fig. 1: Comparison of localization schemes between traditional TDOA and MULoc. (a) Traditional TDOA scheme, (b) MULoc scheme.

are present [28]. To address this, the TDOA scheme reduces collisions using the *tag overhearing* (TO) mechanism. As shown in Fig. 1a, anchors in TDOA systems are synchronized by a global clock and sequentially broadcast ranging packets. Tags overhear these packets and use one-way ranging to calculate the ToF from each anchor. To eliminate clock skew, tags compute the ToF differences among different anchors and determine their own locations through trilateration.

Since the tags listen passively and transmit no packets, TDOA can theoretically support an unlimited number of tags. However, two fundamental limitations still exist. First, the ToF estimation of commercial UWB modules typically suffers from a large deviation of over 150 ps [43], resulting in merely centimeter-level localization accuracy in current TDOA systems [24]. Although UWB phase can provide finer distance estimation, its inherent time-varying offset caused by transmitter-receiver separation (*e.g.*, CFO) cannot be corrected using only TO estimates. Additionally, TDOA requires tight synchronization (*e.g.*, wired or GPSDO [44]) between anchors, which may significantly increase deployment complexity and cost.

MULoc scheme. MULoc addresses the issues mentioned above by introducing a novel mechanism called *anchor overhearing* (AO). Unlike the traditional TDOA scheme where anchors only transmit ranging packets, in MULoc, anchors remain listening after transmission, allowing them to overhear packets from other anchors. As illustrated in Fig. 1b, the ranging packets sent by anchors 1 and 2 are simultaneously received by the tag and anchor 3 (the reference anchor) through TO and AO, respectively. Both the tag and the reference estimate ToF and phase-of-arrival (PoA) from these receptions. Our derivations reveal that the errors in ToF and phase estimates caused by transmitter-receiver separation can be canceled out through a dedicate difference operation between the TO and AO estimates. This provides two unique advantages for MULoc. First, it enables the use of phase estimates in distributed anchor scenarios, which can provide a finer-grained distance measurement. Second, it eliminates the need for synchronization between anchors, significantly simplifying deployment especially in large-scale scenarios. We will detail MULoc's signal processing algorithms in Section III, IV, and present our anchor scheduling scheme in Section V.

B. Signal Processing Pipeline

Fig. 2 shows MULoc's signal processing pipeline, which includes two main modules: 1) **UWB signal recovery**. This module remove the errors in the raw UWB signal by employing a signal difference between the TO and AO estimates. 2) **Fine-grained tag localization**. In this module, we first acquire unambiguous distance difference estimation with millimeter-level accuracy through robust phase ambiguity resolution. Then, a trilateration-based method is employed to calculate the tags' fine-grained locations.

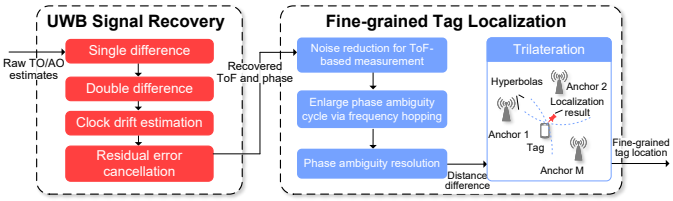

Fig. 2: MULoc's signal processing pipeline.

III. UWB Signal Recovery

In this section, we model the UWB signal and introduce how to eliminate errors caused by device separation and recover accurate ToF and phase estimates.

A. Modeling Raw UWB Signal

We begin by modeling the raw ToF and phase estimates extracted from TO receptions. According to the IEEE 802.15.4 standard [45], commercial UWB devices such as DW1000 use a short-duration pulse of only 2 ns as their baseband waveform, resulting in a large absolute bandwidth of 500 MHz. This enables UWB receivers to distinguish the direct path signal from multipath reflections in the channel impulse response (CIR) profile and estimate its ToF and phase.

Without loss of generality, we consider a localization system with M UWB anchors and one tag, where the anchor 1 through M sequentially send localization packets. The tag receives these packets and extracts raw ToF and phase estimations via tag overhearing (TO).

ToF estimate. Let $d_{i,\text{tag}}$ represent the distance between anchor i and the tag, a UWB packet from anchor i reaches the tag after a propagation delay $\tau_{i,\text{tag}} = d_{i,\text{tag}}/c$. However, hardware imperfections in UWB modules, including oscillator clock drift (δ), initial clock skew after device startup (ΔT), and antenna delay (ψ), introduce additional time delays in the ToF estimate. Taking these errors into account, the raw ToF estimate $r_{i,\text{tag}}$ for TO reception can be modeled as:

$$\begin{aligned} r_{i,\text{tag}} &= \tau_{i,\text{tag}} + \delta_{\text{tag}} t_{i,\text{tag}} - \delta_i t_i + \Delta T_{\text{tag}} - \Delta T_i + \psi_{\text{tag}} - \psi_i \\ &\approx \tau_{i,\text{tag}} + \underbrace{(\delta_{\text{tag}} - \delta_i)\, t_i}_{\text{Time varying skew}} + \underbrace{\Delta T_{\text{tag}} - \Delta T_i}_{\text{Initial skew}} + \underbrace{\psi_{\text{tag}} - \psi_i}_{\text{Antenna delay}}, \end{aligned} \tag{1}$$

where t_i and $t_{i,\text{tag}}$ denote the transmitting and receiving timestamps of the ranging packets, respectively. The subscript i and tag indicate the errors introduced by anchor i and tag. Since the clock drifts δ_{tag} and δ_i are temperature-sensitive, they result in time-varying clock skew in $r_{i,\text{tag}}$. In Eq. 1, we approximate $\delta_{\text{tag}} t_{i,\text{tag}} \approx \delta_{\text{tag}} t_i$ due to the small duration between packet transmission and reception (*e.g.*, less than 100 ns).

Phase estimate. The raw phase estimate $\phi_{i,\text{tag}}$ between anchor i and the tag includes both the actual phase shift corresponding to the propagation delay $\tau_{i,\text{tag}}$ and hardware-related errors, which can be modeled as:

$$\phi_{i,\text{tag}} = [-2\pi f_c \tau_{i,\text{tag}} - \underbrace{2\pi f_c\, (\delta_{\text{tag}} - \delta_i)\, t_i}_{\text{CFO}} - \underbrace{\phi^{\text{tag}}_{\text{ini}} + \phi^{i}_{\text{ini}}}_{\text{Initial offset}} - \underbrace{\phi^{\text{tag}}_{\text{ant}} + \phi^{i}_{\text{ant}}}_{\text{Antenna offset}}] \bmod 2\pi, \tag{2}$$

where f_c is the center frequency of UWB (*e.g.*, 3.5 GHz for channel 1). ϕ_{ini} and ϕ_{ant} represent the initial offset and antenna offset of the UWB devices, respectively. The clock drift δ_i and δ_{tag} contribute to the CFO term, resulting in a time-varying phase drift in $\phi_{i,\text{tag}}$.

The representations of Eq. 1 and Eq. 2 show that the sources of errors in raw ToF and phase estimate are mainly three-fold: time-varying errors, initial errors after device startup, and antenna-related errors. As illustrated in Fig. 3a, the raw ToF exhibits a large bias of over 2 ms, while the phase is corrupted by random noise within $[0, 2\pi]$. Therefore, an error elimination method is required before using these estimates for localization.

B. Error Cancellation using Anchor Overhearing Estimates

To mitigate errors in raw UWB signals, previous studies have explored using bi-directional packets between anchors and tags, which share the same propagation delay but exhibit opposite errors [39, 40, 42]. However, this approach is not feasible in MULoc, as the tags in our system only listen passively and do not transmit. This prevents the use of bi-directional packets for error cancellation.

Instead of using bi-directional UWB packets, MULoc achieves fine-grained error cancellation based on the key observation that the anchor overhearing (AO) estimates in MULoc share the same errors related to anchor i with TO estimates. This allows us to perform error cancellation through a difference operation between the TO and AO estimates.

Single difference. Suppose we choose one anchor, *ref* ($ref \neq i$), to serve as the reference, which overhears packets sent from anchor i. Similar to TO, the AO estimates for ToF ($r_{i,\text{ref}}$) and phase ($\phi_{i,\text{ref}}$) can be expressed as:

$$r_{i,\text{ref}} = \tau_{i,\text{ref}} + \underbrace{(\delta_{\text{ref}} - \delta_i) t_i}_{\text{Time varying skew}} + \underbrace{\Delta T_{\text{ref}} - \Delta T_i}_{\text{Initial skew}} + \underbrace{\psi_{\text{ref}} - \psi_i}_{\text{Antenna delay}}, \tag{3}$$

$$\phi_{i,\text{ref}} = [-2\pi f_c \tau_{i,\text{ref}} - \underbrace{2\pi f_c (\delta_{\text{ref}} - \delta_i) t_i}_{\text{CFO}} - \underbrace{\phi^{\text{ref}}_{\text{ini}} + \phi^{i}_{\text{ini}}}_{\text{Initial offset}} - \underbrace{\phi^{\text{ref}}_{\text{ant}} + \phi^{i}_{\text{ant}}}_{\text{Antenna offset}}] \bmod 2\pi, \tag{4}$$

where the subscript *ref* denotes errors associated with the reference. By comparing TO ($r_{i,\text{tag}}$, $\phi_{i,\text{tag}}$) and AO ($r_{i,\text{ref}}$, $\phi_{i,\text{ref}}$) estimates, we observe that they share error components related to anchor i, such as δ_i, ΔT_i, ψ_i, ϕ^i_{ini}, and ϕ^i_{ant}. Thus, a *single difference (SD)* between these estimates can eliminate the common errors, as illustrated in Fig. 4a.

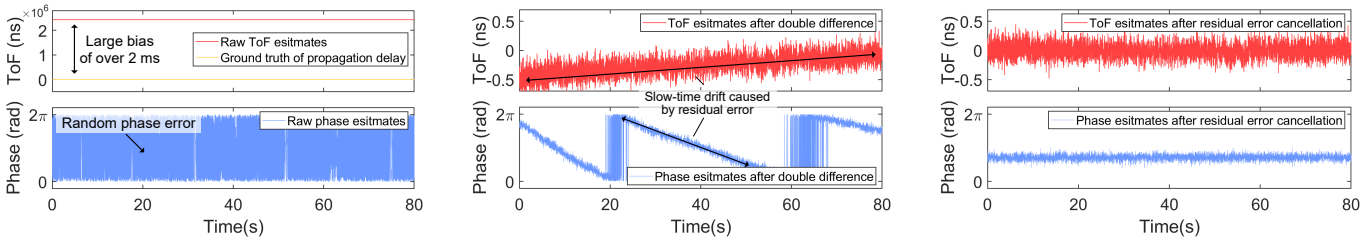

(a) Raw UWB signal before error cancellation (b) Result of double difference (c) Result of residual error cancellation

Fig. 3: Illustration of UWB signal recovery. The raw data are collected from commercial UWB modules.

Given the raw ToF estimates $r_{i,\text{tag}}$ and $r_{i,\text{ref}}$, their single difference result can be initially calculated as:

$$\begin{aligned} r_{i,\text{tag}} - r_{i,\text{ref}} &= \tau_{i_{\text{tag}}} + (\delta_{\text{tag}} - \cancel{\delta_i})t_i + \Delta T_{\text{tag}} - \cancel{\Delta T_i} + \psi_{\text{tag}} - \cancel{\psi_i} \\ &\quad - \tau_{i,\text{ref}} - (\delta_{\text{ref}} - \cancel{\delta_i})t_i - \Delta T_{\text{ref}} + \cancel{\Delta T_i} - \psi_{\text{ref}} + \cancel{\psi_i} \\ &= \tau_{i,\text{tag}} - \tau_{i,\text{ref}} + (\delta_{\text{tag}} - \delta_{\text{ref}})t_i + \Delta T_{\text{tag}} - \Delta T_{\text{ref}} + \psi_{\text{tag}} - \psi_{\text{ref}}. \end{aligned} \tag{5}$$

Suppose the distance $d_{i,\text{ref}}$ between anchor i and reference is known, $\tau_{i,\text{ref}}$ can be compensated as $\tau_{i,\text{ref}} = d_{i,\text{ref}}/c$. The compensated single difference result for ToF r_i^{SD} is:

$$r_i^{\text{SD}} = \tau_{i,\text{tag}} + \underbrace{(\delta_{\text{tag}} - \delta_{\text{ref}})t_i}_{\text{Time varying skew}} + \underbrace{\Delta T_{\text{tag}} - \Delta T_{\text{ref}}}_{\text{Initial skew}} + \underbrace{\psi_{\text{tag}} - \psi_{\text{ref}}}_{\text{Antenna delay}}. \tag{6}$$

The single difference of phase estimate is then derived, and it can be calculated by initially subtracting $\phi_{i,\text{tag}}$ and $\phi_{i,\text{ref}}$ as:

$$\begin{aligned} &\phi_{i,\text{tag}} - \phi_{i,\text{ref}} \\ &= [-2\pi f_c(\tau_{i,\text{tag}} - \tau_{i,\text{ref}}) - 2\pi f_c(\delta_{\text{tag}} - \delta_{\text{ref}})t_i - \phi_{\text{ini}}^{\text{tag}} + \phi_{\text{ini}}^{\text{ref}} - \phi_{\text{ant}}^{\text{tag}} + \phi_{\text{ant}}^{\text{ref}}] \bmod 2\pi. \end{aligned} \tag{7}$$

After compensating $\tau_{i,\text{ref}}$, the single difference result for phase ϕ_i^{SD} becomes:

$$\phi_i^{\text{SD}} = [-2\pi f_c \tau_{i,\text{tag}} - \underbrace{2\pi f_c(\delta_{\text{tag}} - \delta_{\text{ref}})t_i}_{\text{CFO}} - \underbrace{\phi_{\text{ini}}^{\text{tag}} + \phi_{\text{ini}}^{\text{ref}}}_{\text{Initial offset}} - \underbrace{\phi_{\text{ant}}^{\text{tag}} + \phi_{\text{ant}}^{\text{ref}}}_{\text{Antenna offset}}] \bmod 2\pi. \tag{8}$$

Note that the errors related to anchor i are eliminated in Eq. 6 and Eq. 8. Although there still exists errors related to the reference and tag, we observe that these errors are consistent across the single difference results computed using different transmitting anchors, as shown in Fig. 4b. This consistency enables further error reduction through a *double difference (DD)* operation between these single difference results.

Double difference. Considering another UWB packet sent from anchor j ($j \neq i \neq ref$), both the tag and reference overhear this packet, allowing them to compute the single difference for ToF and phase estimates, which can be denoted as r_j^{SD} and ϕ_j^{SD}, respectively. The double difference of the ToF estimate $r_{i,j}^{\text{DD}}$ can be calculated as the difference between r_i^{SD} and r_j^{SD}:

$$\begin{aligned} r_{i,j}^{\text{DD}} = r_i^{\text{SD}} - r_j^{\text{SD}} &= \tau_{i,\text{tag}} + (\delta_{\text{tag}} - \delta_{\text{ref}})t_i + \cancel{\Delta T_{\text{tag}}} - \cancel{\Delta T_{\text{ref}}} + \cancel{\psi_{\text{tag}}} - \cancel{\psi_{\text{ref}}} \\ &\quad - \tau_{j,\text{tag}} - (\delta_{\text{tag}} - \delta_{\text{ref}})t_j - \cancel{\Delta T_{\text{tag}}} + \cancel{\Delta T_{\text{ref}}} - \cancel{\psi_{\text{tag}}} + \cancel{\psi_{\text{ref}}} \\ &= \tau_{i,\text{tag}} - \tau_{j,\text{tag}} + \underbrace{(\delta_{\text{tag}} - \delta_{\text{ref}})(t_i - t_j)}_{\text{Residual error}}. \end{aligned} \tag{9}$$

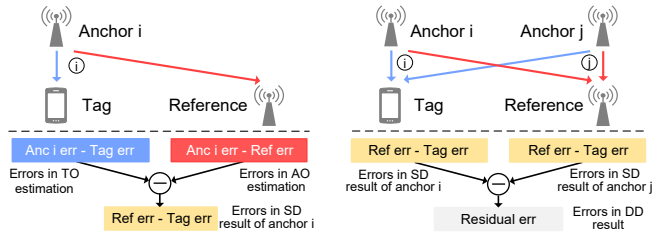

(a) Single difference (SD) (b) Double difference (DD)

Fig. 4: Error cancellation using anchor overhearing estimates.

Similarly, the double difference of the phase estimate $\phi_{i,j}^{\text{DD}}$ is:

$$\phi_{i,j}^{\text{DD}} = \phi_i^{\text{SD}} - \phi_j^{\text{SD}} = [-2\pi f_c(\tau_{i,\text{tag}} - \tau_{j,\text{tag}}) - 2\pi f_c \underbrace{(\delta_{\text{tag}} - \delta_{\text{ref}})(t_i - t_j)}_{\text{Residual error}}] \bmod 2\pi. \tag{10}$$

From Eqs. 9 and 10, we can observe that the random errors due to device startup and antenna delay are completely removed. Additionally, the time-varying errors (*i.e.*, time-varying clock skew and CFO) are also significantly reduced, leaving only a residual error. Fig. 3b shows the double difference results for both ToF and phase estimates. Compared to the raw estimates in Fig. 3a, the large time bias in ToF and random offsets in phase estimates are effectively removed. However, there still exists a slow-time drift due to the residual error term in Eqs. 9 and 10, which should be further eliminated to ensure stable localization performance in MULoc.

C. Residual Error Cancellation

In this subsection, we estimate and remove the residual error from the double difference results. Although the time interval $t_i - t_j$ can be easily calculated as the difference between the transmitting timestamps of the UWB packets, accurately estimating the clock drift difference $\delta_{\text{ref}} - \delta_{\text{tag}}$ is a non-trivial task. This is because the clock drift estimates provided by commercial UWB modules typically suffer from a large variance of over 0.1 part per million (ppm) [46], which is insufficient for fine-grained cancellation.

In MULoc, we achieve precise clock drift estimation by utilizing ranging packets sent from the reference to tag. To inform the tags of the AO estimates for performing the difference operation, the reference regularly send report packets piggybacked with the AO estimates. We observe that the phase

difference between adjacent reporting packets contains fine-grained clock drift information. Consider two report packets sent from the reference at times t_{ref} and $t_{\text{ref}} + \Delta t$, from which we can obtain phase estimates $\phi_{\text{ref,tag}}$ and $\phi'_{\text{ref,tag}}$, respectively. The phase difference $\Delta\phi$ can be calculated as:

$$\begin{aligned}\Delta\phi &= \phi_{\text{ref,tag}} - \phi'_{\text{ref,tag}} \\ &= [-2\pi f_c(\tau_{\text{ref,tag}} - \tau'_{\text{ref,tag}}) + 2\pi f_c(\delta_{\text{tag}} - \delta_{\text{ref}})\Delta t] \bmod 2\pi \\ &\approx [2\pi f_c \underbrace{(\delta_{\text{tag}} - \delta_{\text{ref}})}_{\text{Clock drift difference}} \Delta t] \bmod 2\pi.\end{aligned} \tag{11}$$

Here, we assume that the propagation delay $\tau_{\text{ref,tag}}$ remains constant during the interval Δt, which is about 2.5 ms in MULoc's anchor configuration. With known values of $\Delta\phi$, f_c, and Δt, we can further calculate the clock drift difference $\delta_{\text{tag}} - \delta_{\text{ref}}$ as:

$$\delta_{\text{tag}} - \delta_{\text{ref}} = (\frac{\Delta\phi}{2\pi} + l)\frac{1}{f_c \Delta t}. \tag{12}$$

Due to phase wrapping, the result in Eq. 12 is ambiguous, as it depends on an unknown integer l, which represents the number of $\frac{1}{f_c\Delta t}$ parts contained in $\delta_{\text{tag}} - \delta_{\text{ref}}$. We observe that the clock drift estimates provided by UWB module are coarse but free of ambiguity, and can thus be used to determine the integer l. Let $\widetilde{\delta_{\text{tag}}}$ and $\widetilde{\delta_{\text{ref}}}$ represent the coarse clock drift estimates of UWB module, the integer l can then be computed as:

$$l = \lfloor \frac{\widetilde{\delta_{\text{tag}}} - \widetilde{\delta_{\text{ref}}}}{\frac{1}{f_c\Delta t}} \rfloor = \lfloor (\widetilde{\delta_{\text{tag}}} - \widetilde{\delta_{\text{ref}}}) f_c \Delta t \rfloor, \tag{13}$$

where $\lfloor \cdot \rfloor$ denotes rounding down to the nearest integer. Once l is determined, the unambiguous clock drift difference can be computed using Eq. 12. Our experiments shows that the clock drift differences estimated with this method have a variance of only 0.005 ppm, much lower than the original estimates of UWB modules.

With accurate estimates of clock drift difference $\delta_{\text{ref}} - \delta_{\text{tag}}$, we can multiply it by the time interval $t_i - t_j$ to compute the residual error. Finally, the fine-grained recovered ToF ($r^{\text{rec}}_{i,j}$) and phase ($\phi^{\text{rec}}_{i,j}$) estimates can be derived by subtracting the residual error from the double difference results:

$$r^{\text{rec}}_{i,j} = \tau_{i,\text{tag}} - \tau_{j,\text{tag}}, \tag{14}$$

$$\phi^{\text{rec}}_{i,j} = [-2\pi f_c(\tau_{i,\text{tag}} - \tau_{j,\text{tag}})] \bmod 2\pi. \tag{15}$$

Note that the remaining term in Eqs. 14 and 15 represents the ToF and phase difference caused by different propagation delays of the packets sent from anchor i and j. The recovery results after residual error cancellation are shown in Fig. 3c, where the slow-time drift has been fully removed.

IV. Fine-grained Tag Localization

In this section, we introduce how to achieve fine-grained tag localization by combining the recovered ToF and phase estimates.

A. Phase-based UWB Localization

From the previous section, we have obtained the recovered UWB estimates, reflecting the accurate *propagation delay differences* between packets sent from different anchors. Therefore, it becomes straightforward to apply a TDOA-like trilateration method for tag localization. Trilateration works based on the concept of conic sections. As illustrated in Fig. 5, the distance difference between a tag and two anchors defines a hyperbola, indicating the possible tag locations. With more than two anchors, multiple hyperbolas are obtained, and the tag's position can be determined as the intersection of these hyperbolas.

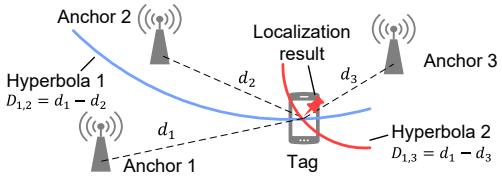

Fig. 5: The basics of trilateration localization.

To achieve millimeter-level localization in MULoc, precise estimates of distance differences is required. Note that both the recovered ToF and phase estimates provide distance difference information. For the ToF estimate $r^{\text{final}}_{i,j}$, the distance difference between anchor i and j can be simply estimated as $D^{\text{ToF}}_{i,j} = c \cdot r^{\text{rec}}_{i,j}$. However, $D^{\text{ToF}}_{i,j}$ typically exhibits an error of around 10 cm due to inaccuracies in ToF estimates.

In comparison, calculating the distance difference from phase estimates is more challenging due to the phase wrapping issue, which can be expressed as:

$$D^{\text{phase}}_{i,j} = c \cdot (\tau_{i,\text{tag}} - \tau_{j,\text{tag}}) = (\frac{\phi^{\text{rec}}_{i,j}}{2\pi} + N_{i,j})\frac{c}{f_c} = (\frac{\phi^{\text{rec}}_{i,j}}{2\pi} + N_{i,j})\lambda, \tag{16}$$

where $N_{i,j}$ is the phase ambiguity number, indicating how many wavelengths λ are contained in $D^{\text{phase}}_{i,j}$. Since both $\phi^{\text{rec}}_{i,j}$ and λ are known, $D^{\text{phase}}_{i,j}$ can be obtained by resolving phase ambiguity $N_{i,j}$. Considering a typical phase noise of 0.3 rad and 3.5 GHz center frequency, $D^{\text{phase}}_{i,j}$ can offer a distance precision of $\frac{0.3\text{rad}}{2\pi} \cdot \frac{3\times10^8\text{m/s}}{3.5\times10^9\text{Hz}} = 0.41$ mm, much better than ToF-based estimation. Therefore, we adopt $D^{\text{phase}}_{i,j}$ as the input of the trilateration algorithm for fine-grained tag localization.

B. Phase Ambiguity Resolution

To resolve the phase ambiguity and obtain accurate estimates of $D^{\text{phase}}_{i,j}$, we note that the ToF-based measurement $D^{\text{ToF}}_{i,j}$ is unambiguous and can thus be used to determine the ambiguity number as $N_{i,j} = \lfloor \frac{D^{\text{ToF}}_{i,j}}{\lambda} \rfloor$ [43]. However, this method faces practical challenge when the error in $D^{\text{ToF}}_{i,j}$ exceeds $\frac{\lambda}{2}$ (*e.g.*, 4.29 cm for 3.5 GHz), which may lead to inaccurate $N_{i,j}$ estimates. Our analysis reveals that the inaccuracy of $D^{\text{ToF}}_{i,j}$ arises from two factors: additive random noise and the tag position-dependent bias. To reduce the additive random noise, we observe that the relative change of $D^{\text{phase}}_{i,j}$ is unambiguous and can provide tag displacement information with millimeter-level accuracy. To address tag position-dependent bias, we note

that commercial UWB modules support frequency hopping across multiple frequencies. This feature allows us to "virtually" enlarge the ambiguity cycle by combining UWB phase estimates from different frequencies, thus avoiding potential errors in ambiguity resolution.

Noise reduction for ToF-based measurement. Now, we combine the accurate displacement information with $D_{i,j}^{\text{ToF}}$ to suppress additive random noise. Let $\phi_{i,j}^{\text{rec}}(k)$ and $\phi_{i,j}^{\text{rec}}(k+1)$ denote the k-th and $(k+1)$-th recovered phase estimates, the tag displacement $\Delta D_{i,j}^{\text{phase}}$ can be calculated as:

$$\Delta D_{i,j}^{\text{phase}}(k) = [\phi_{i,j}^{\text{rec}}(k+1) - \phi_{i,j}^{\text{rec}}(k)]\frac{\lambda}{2\pi}. \tag{17}$$

Note that Eq. 17 is valid when the tag's moving speed is less than $\frac{\lambda}{2\Delta t}$ [34], where Δt denotes the interval between two localization estimates. With MULoc's short localization interval of 2.5 ms, this threshold corresponds to a maximum moving speed of $\frac{8.57 \text{ cm}}{2\times 2.5 \text{ ms}} \approx 17.14$ m/s, which is more than sufficient for most sensing applications such as human tracking. To verify the accuracy of the obtained displacement, we place the tag on a high-precision sliding track and move it with a known displacement. The recovered displacement is shown in Fig. 6a, and it closely matches the ground truth.

With the accurate displacement $\Delta D_{i,j}^{\text{phase}}(k)$ obtained, we can then fuse it with $D_{i,j}^{\text{ToF}}$ using:

$$D_{i,j}^{\text{filt}}(k+1) = \frac{1}{F}D_{i,j}^{\text{ToF}}(k+1) + \frac{F-1}{F}[D_{i,j}^{\text{filt}}(k) + \Delta D_{i,j}^{\text{phase}}(k)], \tag{18}$$

where $D_{i,j}^{\text{filt}}$ represents the filtered distance difference estimates, and F is a user-defined parameter. The rationale behind Eq. 18 is that $D_{i,j}^{\text{ToF}}$ and $D_{i,j}^{\text{phase}}$ should exhibit identical distance change between the k-th and $(k+1)$-th estimates. A larger value of F places more emphasis on the displacement calculated from phase estimates, resulting in better noise suppression. However, this also increases the sensitivity of $D_{i,j}^{\text{filt}}$ to initial estimates, which may contain large errors. Empirically, we find that setting $F = 0.7$ provides a good balance between these effects. Fig. 6b compares the distance estimates of $D_{i,j}^{\text{filt}}$ and $D_{i,j}^{\text{ToF}}$, showing that our filtering method significantly reduces the influence of additive random noise. It is worth noting that the filtered result $D_{i,j}^{\text{filt}}$ still exists the location-dependent distance measurement bias, which may lead to incorrect estimates of phase ambiguity numbers.

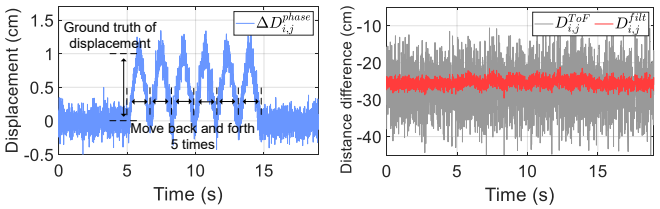

(a) Phase-based accurate tag displacement estimation

(b) Result of fusion-based filtering method

Fig. 6: Noise reduction for ToF-based measurement by fusing it with accurate relative phase change.

Enlarging ambiguity cycle via frequency hopping. We further enlarge the phase ambiguity cycle by performing frequency hopping to acquire the UWB phase at different wavelengths. Prior work [39, 42] employs frequency hopping in two-way ranging systems to enhance robustness in phase ambiguity resolution. In MULoc, we implement frequency hopping by having the anchors and tags switch between ch.1 (3.5 GHz) and ch.3 (4.5 GHz) every two localization rounds. For a commercial DW1000 module, the hopping operation takes around 400 μs. For each frequency, we apply our signal recovery algorithm to obtain the phase estimates, denoted as $\phi_{i,j}^{\text{rec,ch1}}$ and $\phi_{i,j}^{\text{rec,ch3}}$, respectively. With these phase estimates, we can obtain the following system of equations:

$$\begin{cases} \phi_{i.j}^{\text{rec,ch1}} = [\frac{D_{i,j}^{\text{phase}} f_c^{\text{ch1}}}{c}] \bmod 2\pi \\ \phi_{i.j}^{\text{rec,ch3}} = [\frac{D_{i,j}^{\text{phase}} f_c^{\text{ch3}}}{c}] \bmod 2\pi \end{cases}, \tag{19}$$

where $f_c^{\text{ch1}} = 3.5$ GHz and $f_c^{\text{ch3}} = 4.5$ GHz are the center frequencies of UWB ch.1 and ch.3, respectively. The $D_{i,j}^{\text{phase}}$ can then be obtained by solving Eq. 19 as follows:

$$D_{i,j}^{\text{phase}} = (\frac{\phi_{i,j}^{\text{rec,ch1}} - \phi_{i,j}^{\text{rec,ch3}}}{2\pi} + N_{i,j}^{\text{virt}})\lambda_{\text{virt}}, \tag{20}$$

where $\lambda_{\text{virt}} = \frac{c}{f_c^{\text{ch3}} - f_c^{\text{ch1}}} = 30$ cm is the "virtual" wavelength, and $N_{i,j}^{\text{virt}}$ is the new ambiguity number, respectively. The new ambiguity cycle is significantly enlarged compared to using a single frequency, as shown in Fig. 7, which illustrates the equivalent result of using a "virtual" channel with a 1 GHz center frequency. We can now reliably determine the new ambiguity number as $N_{i,j}^{\text{virt}} = \lfloor \frac{D_{i,j}^{\text{filt}}}{\lambda_{\text{virt}}} \rfloor$, even in the presence of centimeter-level distance measurement bias. The accurate $D_{i,j}^{\text{phase}}$ can then be computed using Eq. 20.

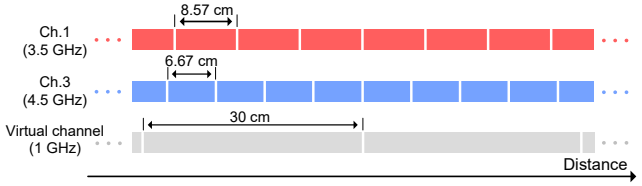

Fig. 7: Enlarging ambiguity cycle via frequency hopping.

C. Localization Method

Now that we have accurate estimates of the distance differences $D_{i,j}^{\text{phase}}$ between anchors, we can proceed to perform precise trilateration for UWB tags. The goal of the trilateration algorithm is to find an optimal location, where the theoretical distance differences closely match our estimates. Given a candidate tag location $\boldsymbol{p}$ and two anchor locations $\boldsymbol{p_i}$ and $\boldsymbol{p_j}$, the theoretical distance differences of the tag to these two anchors can be calculated as:

$$D_{i,j}^{\text{theor}} = ||\boldsymbol{p} - \boldsymbol{p_i}|| - ||\boldsymbol{p} - \boldsymbol{p_j}||. \tag{21}$$

The tag's location is then determined by optimizing the following cost function:

$$\arg\min_{\boldsymbol{p}} \textstyle\sum_{i\neq j}^{M} (D_{i,j}^{\text{theor}} - D_{i.j}^{\text{phase}})^2. \tag{22}$$

In MULoc, we solve Eq. 22 using the well-known Chan's method [37] based on least-squares estimation, which can compromise the localization accuracy and computational cost.

V. Implementation

In this section, we describe the implementation details of MULoc.

A. Hardware Implementation

As shown in Fig. 8, we implement MULoc using a commercial UWB module Jiuling X1 [47], which includes a Decawave DW1000 UWB transceiver and an STM32F103 MCU. The DW1000 transceiver is equipped with a 3-dbi antenna and a low-cost 38.4 MHz TCXO oscillator. We configure the DW1000 to operate on both ch.1 (3.5 GHz) and ch.3 (4.5 GHz), each with a bandwidth of 500 MHz. To increase the location update rate, we use a short preamble length of 64 symbols and the maximum data rate of 6.8 MHz.

We implement both the anchor and tag of MULoc on the same hardware platform. The anchor is powered by a portable charger with no additional wired connection. We connect the tag to a WiFi module ESP32-S3 via USB-CDC. The WiFi module transmits the raw TO and AO estimates to a PC (with an R7-5800H CPU and 16 GB memory) for signal processing. A three-point calibration [35] is applied to mitigate the linear error in ToF and phase estimates.

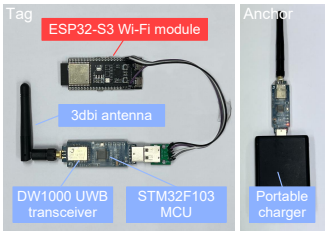

Fig. 8: Hardware implementation.

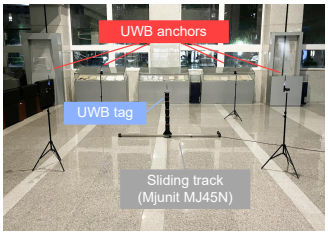

Fig. 9: Experimental setup for evaluation.

B. Software Implementation

We implement the anchor scheduling scheme of MULoc with C and Decawave API [48] on the MCU of the UWB module. For signal processing, we develop and execute the localization algorithms with MATLAB on the PC. Next, we provide details of MULoc's anchor scheduling scheme.

In Section III, we discussed using a fixed anchor *ref* as the reference for signal recovery. While simple, this approach requires an additional anchor, which raises the deployment cost in practical scenarios. To address this issue, MULoc incorporates *reference switching* mechanism. As shown in Fig 10, anchor 1, 2, and 3 send UWB packets at t_1, t_2, and t_3 in sequence, which are overheard by the tag. The interval between these packets is set to 600 μs. After each transmission, all anchors enter a listening state and continue to overhear packets from other anchors. The AO estimates are then be piggybacked in the next round of localization packet and sent to the tag. This scheme enables any anchor to serve as the reference to extract the required AO estimates for signal recovery. For example, to perform double difference between anchors 1 and 2, we can use anchor 3 as the reference. When more than four anchors are present, multiple reference candidates may exist. In practice, we choose the anchor with a smaller index as the reference.

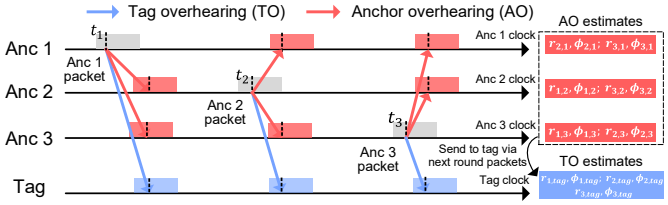

Fig. 10: A three anchor example of MULoc's anchor scheduling scheme.

VI. Evaluation

In this section, we evaluate the performance of MULoc in both single-point localization and trajectory tracking scenarios, with several impact factors considered.

A. Experimental Setup

As shown in Fig. 9, we conduct the evaluation in a typical indoor environment. Four UWB anchors are placed at (0, 0) cm, (0, 315) cm, (360, 315) cm, and (360, 0) cm, with a height of 1.5 m. The location update rate is set to 200 Hz. For single-point localization, we place the tag at different locations in the environment. For tracking scenario, we place the tag on a high-precision sliding track (Mjunit MJ45N) and move it along pre-programmed trajectories.

Ground truth. For single-point localization, we record the precise locations of anchors and tags using two accurate laser rangefinders (SNDWAY-TA70) [49] with 1 mm accuracy. In the trajectory tracking scenario, the sliding track offers a high moving precision of 0.01 mm, and we record the configuration of the sliding track's program as the ground truth. The sliding track's location is also determined using laser rangefinders.

B. Localization Performance

Overall accuracy. As shown in Fig. 11a, we place a UWB tag at 30 different locations to evaluate the overall localization accuracy. We choose a open-sourced TDOA localization system ATLAS [24] as our baseline. Note that the ATLAS system requires an additional anchor as the initiator for time synchronization. To further investigate the importance of phase estimates in MULoc, we develop a simplified version of our system, named MULoc-, which uses only the recovered ToF estimates for localization.

Fig. 11b illustrates the overall localization error distribution across 30 tag locations. The results show that our system achieves a median localization error of just 0.47 cm and a 90-th percentile error of 1.02 cm, reducing the error by 91.12% (median) and 89.9% (90-th percentile) compared to the ATLAS system. With most errors eliminated via our novel signal recovery method, the simplified version MULoc- also outperforms ATLAS even without synchronization. However, MULoc- still has a much larger error than MULoc due to the noisy UWB ToF estimates. Additionally, the mean absolute error (MAE) for each tag location is shown in Fig.11c, where

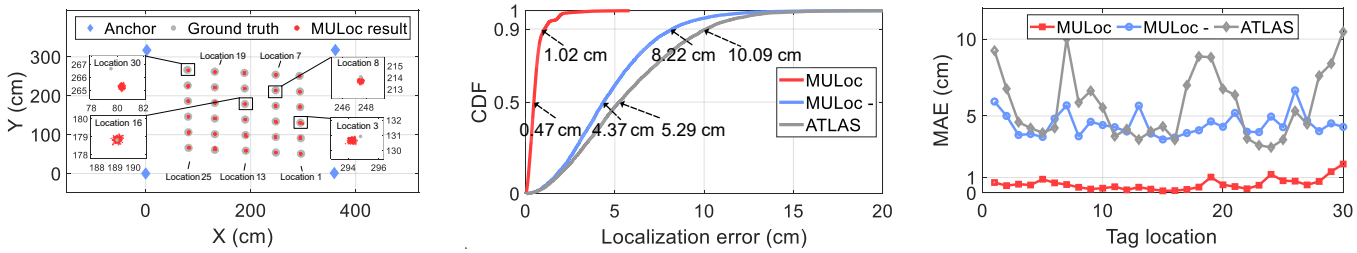

(a) Localization result (b) CDF of localization error (c) Localization error of each tag location

Fig. 11: Overall localization performance.

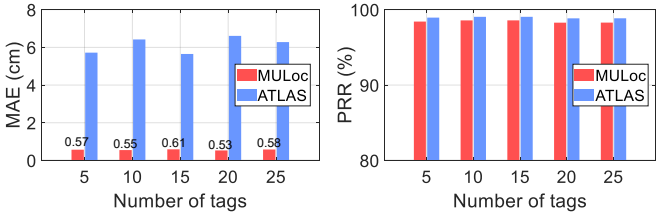

(a) Localization error (b) Packet reception rate

Fig. 12: Performance under large tag numbers.

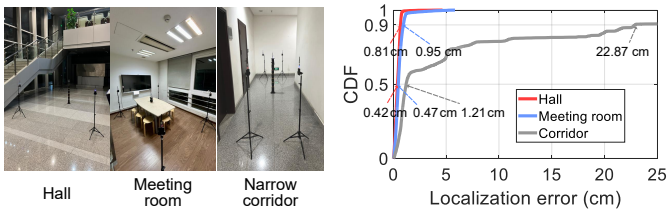

(a) Environments (b) CDF of localization error

Fig. 13: Impact of multipath.

we can observe that MULoc consistently achieves millimeter-level localization error across most tag locations.

Performance under large tag numbers. To support a large number of UWB tags, MULoc avoid packet collisions by using only overheard estimates for localization. In this experiment, we evaluate MULoc's performance in large-scale deployment by placing different numbers of tags (up to 25 tags) in the room. For each configuration, we connect these tags to the PC via UWB-CDC and collect UWB estimates from them. Fig. 12 compares the localization error and packet reception ratio (PRR) of MULoc with those of ATLAS across different numbers of tags. The results show that MULoc achieves a small MAE below 0.6 cm and a high PRR of over 98% even with 25 tags. In contrast, while ATLAS also maintains a high PRR, it has an MAE of about 10 times larger than that of MULoc. These results demonstrate that our system can achieve millimeter-level accurate localization even in large-scale deployment scenarios.

Impact of multipath. MULoc handles multipath with the 500 MHz bandwidth of commercial UWB module, which offers a distance resolution of 60 cm. To investigate it's impact, we deploy MULoc in three distinct indoor environments with varying levels of multipath reflections, including i) a 5×5 m hall with slight multipath, ii) a 3×5 m meeting room with moderate multipath, and iii) a 2×5 m narrow corridor with strong multipath, as shown in Fig. 13a. In each environment, we collect localization results at 10 different locations. The CDF of localization errors is shown in Fig. 13b, showing that MULoc achieves a median error of 0.42 cm in the hall and 0.47 cm in the meeting room. However, a large 90-th percentile error of 22.87 cm is observed in the narrow corridor scenario. We attribute this large error to the distortion of ToF estimates caused by strong multipath reflections from walls, which may lead to inaccuracies in phase ambiguity resolution.

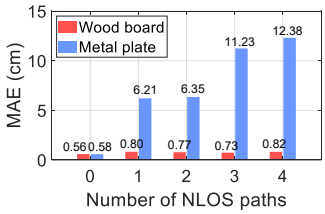

Fig. 14: Impact of NLOS.

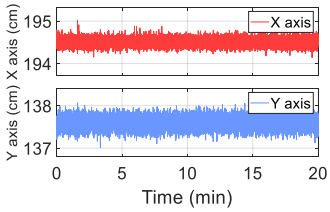

Fig. 15: Long-term stability.

Impact of NLOS. To study the impact of non-line-of-sight (NLOS) conditions on our system, we construct scenarios using common indoor materials (*i.e.*, wooden boards and metal plates in sizes of 70×70 cm) as obstacles. In each scenario, we evaluate the localization accuracy with a varying number of LOS paths blocked. As illustrated in Fig. 14, the MAE increases slightly from 0.56 cm to 0.82 cm when 4 anchors are obstructed by wooden boards, which is comparable to the result of LOS conditions. This indicates that MULoc is robust against typical NLOS conditions found in indoor environments. However, when all LOS paths are blocked by metal plates, we observe a large increase in error of up to 12.38 cm. We attribute this large error to incorrect first path estimations by the UWB module, which leads to a significant bias on ToF and phase estimates. Fortunately, such severe NLOS conditions are not common and can be avoided by placing anchors away from metal obstacles.

Long-term stability. Next, we evaluate the long-term stability of localization accuracy. In MULoc, we deal with time-varying errors through a novel error cancellation method. To verify this, we collect localization data for 20 minutes. The localization results of the x-axis and y-axis are illustrated in Fig. 15, indicating that MULoc exhibits no long-term drift.

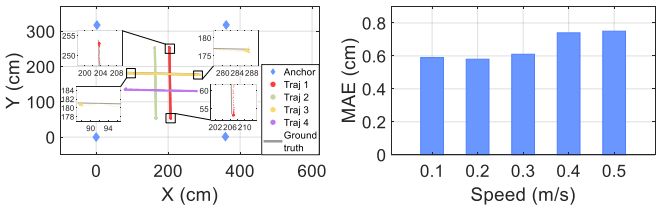

(a) Tracking result (b) Impact of tag speed

Fig. 16: Tracking pre-defined trajectories.

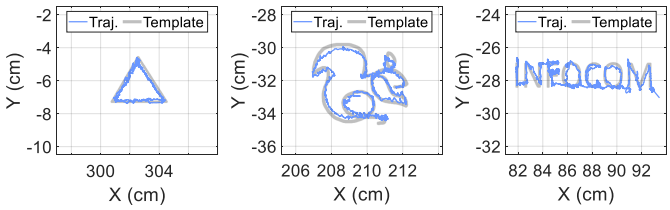

(a) User 1: a triangle (b) User 2: a squirrel (c) User 3: "INFOCOM"

Fig. 17: Tracking arbitrary handwriting of multiple users.

C. Trajectory Tracking Performance

Pre-defined trajectories. We evaluate the overall tracking performance of MULoc by placing the sliding track at four different locations in the room. For each setup, we move the tag along the sliding track for a distance of 2 m at a constant speed of 0.1 m/s. Fig. 16a illustrates the tracking results of MULoc alongside the ground truths for the four trajectories. Our system demonstrates an overall MAE of only 0.59 cm. We further explore the impact of varying tag speeds on tracking accuracy by gradually increasing the speed from 0.1 m/s to 0.5 m/s (the maximum speed of the sliding track). As depicted in Fig. 16b, the MAE slightly increases from 0.59 cm to 0.68 cm as the speed increases, indicating that MULoc consistently provides mm-level tag accuracy at varying moving speeds.

Arbitrary trajectories. To showcase MULoc's capability in tracking arbitrary trajectories, we recruit three volunteers to perform handwriting while holding tags. Fig. 17 illustrates the tracking results for different users, including two images (a triangle and a squirrel) and a word ("INFOCOM"). The trajectories are smoothed with a Savitzky-Golay filter. Experimental results show that MULoc can achieve high accuracy trajectory tracking for complex strokes and small characters as tiny as 2×2 cm.

VII. Related Work

RF-based localization. In the past decade, the field of indoor localization using wireless signals such as WiFi [5–14], RFID [15–17], and UWB [23–35] has received much attention. For instance, to achieve accurate time-based WiFi localization, Splicer [9] enables precise power-delay profiling by performing frequency hopping across several WiFi channels. By fusing the ToF and PDOA estimates, SpotFi [8] achieves super-resolution AOA estimation on commercial WiFi devices. However, due to the limited bandwidth (*e.g.*, 80 MHz) on commercial devices [50], WiFi-based solutions suffer from large inaccuracies of several decimeters, which do not satisfy the high precision requirements in many sensing applications such as gesture tracking. Benefiting from the mono-static design of where the transmitter and receiver are synchronized, RFID readers can provide accurate phase estimates with a precision of 0.0015 rad [16]. Using the accurate phase estimates, RF-IDraw [15] achieves cm-level tracking for human gestures. By proposing the differential augmented hologram (DAH) method, Tagoram [16] further pushes the tracking accuracy to mm-level on commercial RFID devices. Despite these advances, the high cost of over $1000 for RFID readers limits their broader adoption [51].

UWB-based localization. In contrast to the aforementioned technologies, UWB-based localization systems are becoming increasingly popular owing to their stable performance and moderate hardware price [22]. Leveraging the ps-level timestamp resolution of UWB, early systems mainly utilize a TWR for localization [23, 27, 52, 53]. However, the large amount of packet exchanges in the TWR scheme leads to a reduced location update rate and small tag capacity [28]. To address these issues, many current systems employ TDOA [24–26] or AOA [30–33, 35] schemes to enhance location update rate and tag capacity. However, the localization accuracy of these systems is still constrained to centimeter-level due to the limited precision of ToF and AOA estimates on commercial UWB modules. Some recent work attempts to enhance accuracy by combining these schemes. ITrackU [34] achieves mm-level relative tracking for a single tag by combining the TDOA and relative change of PDOA measurements. However, it requires additional hardware modification and does not support absolute localization. By using bi-directional messages, one recent work [42] achieves millimeter-level ranging between UWB devices. Nevertheless, it supports the localization for only a few tags with a low update rate. To our best knowledge, none of the existing work can localize a large number of UWB tags with millimeter-level accuracy.

VIII. Conclusion

This paper presents MULoc, the first system that can localize an unlimited number of tags with mm-level accuracy. By introducing the novel anchor overhearing (AO) approach, we enable the use of phase estimates in practical localization scenarios. To address errors in raw UWB signals, we propose a signal-difference-based processing pipeline that combines TO and AO estimates. MULoc achieves robust phase ambiguity resolution through fusion-based filtering and frequency hopping. Experimental results demonstrate that MULoc achieves a median localization error of 0.47 cm and 90% error of 1.02 cm. We believe that our proposed techniques will play an important role in future large-scale, high-precision UWB applications. In our future work, we aim to further enhance MULoc by improving its robustness in larger localization areas, more complex multipath environments, and optimizing the localization latency. The authors have provided public access to their code at: https://github.com/MULoc.

REFERENCES

[1] K. Niu, F. Zhang, X. Wang, Q. Lv, H. Luo, and D. Zhang, "Understanding wifi signal frequency features for position-independent gesture sensing," *IEEE Transactions on Mobile Computing*, vol. 21, no. 11, pp. 4156–4171, 2021.

[2] A. Wang and S. Gollakota, "Millisonic: Pushing the limits of acoustic motion tracking," in *ACM CHI*, 2019, pp. 1–11.

[3] Y. Cao, A. Dhekne, and M. Ammar, "Utrack3d: 3d tracking using ultra-wideband (uwb) radios," in *ACM MobiSys*, 2024, pp. 345–358.

[4] M. Borges, A. Symington, B. Coltin, T. Smith, and R. Ventura, "Htc vive: Analysis and accuracy improvement," in *IEEE IROS*, 2018, pp. 2610–2615.

[5] P. Bahl and V. N. Padmanabhan, "Radar: An in-building rf-based user location and tracking system," in *IEEE INFOCOM*, vol. 2, 2000, pp. 775–784.

[6] C. Wu, Z. Yang, Y. Liu, and W. Xi, "Will: Wireless indoor localization without site survey," *IEEE Transactions on Parallel and Distributed systems*, vol. 24, no. 4, pp. 839–848, 2012.

[7] J. Xiong and K. Jamieson, "{ArrayTrack}: A {Fine-Grained} indoor location system," in *USENIX NSDI*, 2013, pp. 71–84.

[8] M. Kotaru, K. Joshi, D. Bharadia, and S. Katti, "Spotfi: Decimeter level localization using wifi," in *ACM SIGCOMM*, 2015, pp. 269–282.

[9] Y. Xie, Z. Li, and M. Li, "Precise power delay profiling with commodity wifi," in *ACM MobiCom*, 2015, pp. 53–64.

[10] X. Li, D. Zhang, Q. Lv, J. Xiong, S. Li, Y. Zhang, and H. Mei, "Indotrack: Device-free indoor human tracking with commodity wi-fi," *ACM IMWUT*, vol. 1, no. 3, pp. 1–22, 2017.

[11] K. Qian, C. Wu, Y. Zhang, G. Zhang, Z. Yang, and Y. Liu, "Widar2. 0: Passive human tracking with a single wi-fi link," in *ACM MobiSys*, 2018, pp. 350–361.

[12] Y. Xie, J. Xiong, M. Li, and K. Jamieson, "md-track: Leveraging multi-dimensionality for passive indoor wi-fi tracking," in *ACM MobiCom*, 2019, pp. 1–16.

[13] J. Ni, F. Zhang, J. Xiong, Q. Huang, Z. Chang, J. Ma, B. Xie, P. Wang, G. Bian, X. Li, and C. Liu, "Experience: Pushing indoor localization from laboratory to the wild," in *ACM MobiCom*, 2022, p. 147–157.

[14] G. Chi, Z. Yang, J. Xu, C. Wu, J. Zhang, J. Liang, and Y. Liu, "Wi-drone: wi-fi-based 6-dof tracking for indoor drone flight control," in *ACM MobiSys*, 2022, pp. 56–68.

[15] J. Wang, D. Vasisht, and D. Katabi, "Rf-idraw: Virtual touch screen in the air using rf signals," *ACM SIGCOMM CCR*, vol. 44, no. 4, pp. 235–246, 2014.

[16] L. Yang, Y. Chen, X.-Y. Li, C. Xiao, M. Li, and Y. Liu, "Tagoram: Real-time tracking of mobile rfid tags to high precision using cots devices," in *ACM MobiCom*, 2014, pp. 237–248.

[17] J. Liu, F. Zhu, Y. Wang, X. Wang, Q. Pan, and L. Chen, "Rf-scanner: Shelf scanning with robot-assisted rfid systems," in *IEEE INFOCOM*. IEEE, 2017, pp. 1–9.

[18] C. Peng, G. Shen, Y. Zhang, Y. Li, and K. Tan, "Beepbeep: a high accuracy acoustic ranging system using cots mobile devices," in *ACM SenSys*, 2007, pp. 1–14.

[19] W. Mao, J. He, and L. Qiu, "Cat: high-precision acoustic motion tracking," in *ACM MobiCom*, 2016, pp. 69–81.

[20] L. Wang, H. Wan, T. Zhao, K. Sun, S. Shi, H. Dai, G. Chen, H. Liu, and W. Wang, "Scalar: Self-calibrated acoustic ranging for distributed mobile devices," *IEEE Transactions on Mobile Computing*, 2023.

[21] W. Mao, W. Sun, M. Wang, and L. Qiu, "Deeprange: Acoustic ranging via deep learning," *ACM IMWUT*, vol. 4, no. 4, pp. 1–23, 2020.

[22] F. Zhang, Z. Chang, J. Xiong, J. Ma, J. Ni, W. Zhang, B. Jin, and D. Zhang, "Embracing consumer-level uwb-equipped devices for fine-grained wireless sensing," *ACM IMWUT*, vol. 6, no. 4, pp. 1–27, 2023.

[23] B. Kempke, P. Pannuto, B. Campbell, and P. Dutta, "Surepoint: Exploiting ultra wideband flooding and diversity to provide robust, scalable, high-fidelity indoor localization," in *ACM SenSys*, 2016, pp. 137–149.

[24] J. Tiemann and C. Wietfeld, "Scalable and precise multi-uav indoor navigation using tdoa-based uwb localization," in *IPIN*. IEEE, 2017, pp. 1–7.

[25] B. Großwindhager, M. Stocker, M. Rath, C. A. Boano, and K. Römer, "Snaploc: An ultra-fast uwb-based indoor localization system for an unlimited number of tags," in *ACM/IEEE IPSN*, 2019, pp. 61–72.

[26] P. Corbalán, G. P. Picco, and S. Palipana, "Chorus: Uwb concurrent transmissions for gps-like passive localization of countless targets," in *ACM/IEEE IPSN*, 2019, pp. 133–144.

[27] A. Dhekne, A. Chakraborty, K. Sundaresan, and S. Rangarajan, "{TrackIO}: Tracking first responders {Inside-Out}," in *USENIX NSDI*, 2019, pp. 751–764.

[28] J. Yang, B. Dong, and J. Wang, "Vuloc: Accurate uwb localization for countless targets without synchronization," *ACM IMWUT*, vol. 6, no. 3, pp. 1–25, 2022.

[29] F. Shan, H. Huo, J. Zeng, Z. Li, W. Wu, and J. Luo, "Ultra-wideband swarm ranging protocol for dynamic and dense networks," *IEEE/ACM Transactions on Networking*, vol. 30, no. 6, pp. 2834–2848, 2022.

[30] I. Dotlic, A. Connell, H. Ma, J. Clancy, and M. McLaughlin, "Angle of arrival estimation using decawave dw1000 integrated circuits," in *IEEE WPNC*, 2017, pp. 1–6.

[31] M. Gowda, A. Dhekne, S. Shen, R. R. Choudhury, L. Yang, S. Golwalkar, and A. Essanian, "Bringing {IoT} to sports analytics," in *USENIX NSDI*, 2017, pp. 499–513.

[32] M. Heydariaan, H. Dabirian, and O. Gnawali, "Anguloc: Concurrent angle of arrival estimation for indoor localization with uwb radios," in *IEEE DCOSS*, 2020, pp. 112–119.

[33] M. Zhao, T. Chang, A. Arun, R. Ayyalasomayajula, C. Zhang, and D. Bharadia, "Uloc: Low-power, scalable and cm-accurate uwb-tag localization and tracking for indoor applications," *ACM IMWUT*, vol. 5, no. 3, pp. 1–31, 2021.

[34] Y. Cao, A. Dhekne, and M. Ammar, "Itracku: tracking a pen-like instrument via uwb-imu fusion," in *ACM MobiSys*, 2021, pp. 453–466.

[35] A. Arun, S. Saruwatari, S. Shah, and D. Bharadia, "Xrloc: Accurate uwb localization for xr systems," in *ACM SenSys*, 2023.

[36] Z. Chang, F. Zhang, J. Xiong, X. Xue, Z. Wang, B. Jouaber, and D. Zhang, "Uwbori: Enabling accurate orientation estimation with ultra-wideband signals," in *IEEE Smart World Congress (SWC)*, 2024.

[37] T. F. Chan, G. H. Golub, and P. Mulet, "A nonlinear primal-dual method for total variation-based image restoration," *SIAM journal on scientific computing*, vol. 20, no. 6, pp. 1964–1977, 1999.

[38] T. Wang, H. Zhao, and Y. Shen, "An efficient single-anchor localization method using ultra-wide bandwidth systems," *Applied Sciences*, vol. 10, no. 1, p. 57, 2019.

[39] D. Vasisht, S. Kumar, and D. Katabi, "{Decimeter-Level} localization with a single {WiFi} access point," in *USENIX NSDI*, 2016, pp. 165–178.

[40] J. Jiang, J. Wang, Y. Chen, Y. Liu, and Y. Liu, "Locra: Enable practical long-range backscatter localization for low-cost tags," in *ACM MobiSys*, 2023, pp. 317–329.

[41] Y. Schröder and L. Wolf, "Inphase: Phase-based ranging and localization," *ACM Transactions on Sensor Networks*, vol. 18, no. 2, pp. 1–39, 2022.

[42] J. Ma, F. Zhang, B. Jin, C. Su, S. Li, Z. Wang, and J. Ni, "Push the limit of highly accurate ranging on commercial uwb devices," *ACM IMWUT*, vol. 8, no. 2, pp. 1–27, 2024.

[43] A. Dhekne, M. Gowda, Y. Zhao, H. Hassanieh, and R. R. Choudhury, "Liquid: A wireless liquid identifier," in *ACM MobiSys*, 2018, pp. 442–454.

[44] Ettus, "Gpsdo," https://www.ettus.com/all-products/gpsdo-mini/.

[45] IEEE, "Ieee 802.15.4-2020-ieee standard for low-rate wireless networks," https://standards.ieee.org/ieee/802.15.4/7029/, 2020.

[46] J. Krška and V. Navrátil, "Utilization of carrier-frequency offset measurements in uwb tdoa positioning with receiving tag," *Sensors*, vol. 23, no. 5, p. 2595, 2023.

[47] "Jiuling x1 pro," https://www.aliexpress.com/i/1005004399526480.html, 2023.

[48] Qorvo, "Dw1000 soft api guide," https://www.qorvo.com/products/d/da008000, 2016.

[49] SNDWAY, "Sndway laser rangefinder," https://sndway.co/, 2017.

[50] C. Chen, H. Song, Q. Li, F. Meneghello, F. Restuccia, and C. Cordeiro, "Wi-fi sensing based on ieee 802.11 bf," *IEEE Communications Magazine*, vol. 61, no. 1, pp. 121–127, 2022.

[51] impinj, "Speedway r420," https://www.impinj.com/products/readers/impinj-speedway, 2024.

[52] C. Su, F. Zhang, B. Jin, J. Ma, J. Ni, S. Li, and Z. Wang, "Uwbloc: Nlos mitigation for practical uwb localization," in *2023 IEEE Smart World Congress (SWC)*. IEEE, 2023, pp. 1–8.

[53] Y. Chen, J. Wang, and J. Yang, "Exploiting anchor links for nlos combating in uwb localization," *ACM Transactions on Sensor Networks*, vol. 20, no. 3, pp. 1–22, 2024.